Geoscience Letters

RESEARCH LETTER

Open Access

Holocene loess in the Himalayas piedmont of southeastern Nepal

Edgardo M. Latrubesse[1*] and Abang M. S. Nugraha[2*]

Abstract

Loess, loess-like, sandy loess, and sandy-silty fluvial–aeolian deposits are intercalated to fluvial sediments and lie on a flat surface under intense agricultural land use in Bardibas, Mahottari district, central Nepal. To identify the depositional processes and provenance, we carried out geochemical, mineralogical, SEM, and grain-size analyses. Optically stimulated luminescence (OSL) dating shows the aeolian deposits are from the late Holocene (1.0–4.8 ka). Our results demonstrate that the loess and loess-like deposits (i) were dominantly sourced locally from deflation Quaternary sediments of the Terai Plain; (ii) are related to the composition of Siwalik rocks; and (iii) were deposited during dry periods of weak activity of the Indian Summer Monsoon.

Keywords Loess, Nepal, Holocene, Himalaya

Introduction

For decades, Asian loess deposits in China and the Tibetan Plateau have been used as a main proxy for paleogeographic and paleoclimatic reconstructions (Heller and Liu 1984; Kukla 1987; Pye 1987; Porter 2001; Sun 2002a, b; Lu et al. 2004; Owen et al. 2006; Sun et al. 2007, Jones and Pal 2009 among many others). The most studied locations with loess in the southwest region of the Himalayas are in the Kashmir region and some from small intramountain areas in the Central Himalayas (India) (Pant 1993; Dodonov and Baiguzina 1995; Ahmad and Chandra 2013; Liu et al. 2017; Muhs 2018; Li et al. 2020; Mir et al. 2022). However, loess records from the southeastern flanks and foothills of the Himalayas are less known. To the best of our knowledge, only a couple of articles describe paleosoils and briefly relate them to loess as overlying glacial deposits in the high mountains of eastern Nepal (Guggenberger et al. 1998; Baumler 2001). We are not aware of other published records of Holocene loess from the Himalayan foothills on the Gangetic Plain in Nepal.

Here, we present previously undescribed loess deposits from the Himalayan foothills in central Nepal (Fig. 1). We determine their sedimentological, geochemical, and mineralogical characteristics and their chronology, discuss their provenance, and correlate them with aeolian and other paleoenvironmental proxies in India and Tibet.

Regional setting

We surveyed the piedmont area around Bardibas city (Fig. 1). The geomorphology of the area is characterized by the Lesser Himalayas to the north, and the widespread alluvial Terai Plain to the south, in the Kosi Gandak Interfan area (Sinha et al. 2014), a sub-unit of the foreland Gangetic morpho-sedimentary plain. The height of the Lesser Himalayas in the study area varies between 700 and 1500 m asl., whereas the average elevation of the plain is ~50–100 m asl.

The southwest summer monsoon moves north-westwards and dominates the current climate of central Nepal, bringing summer rainfalls (June–September), with

*Correspondence:
Edgardo M. Latrubesse
latrubesse23@gmail.com
Abang M. S. Nugraha
abang.nugraha@ntu.edu.sg
[1] Federal University of Goiás-UFG, Graduate Program in Environmental Sciences-CIAMB, Campus II, Goiania, GO 74690-900, Brazil
[2] Earth Observatory of Singapore, Nanyang Technological University, 50 Nanyang Ave., Singapore 639798, Singapore

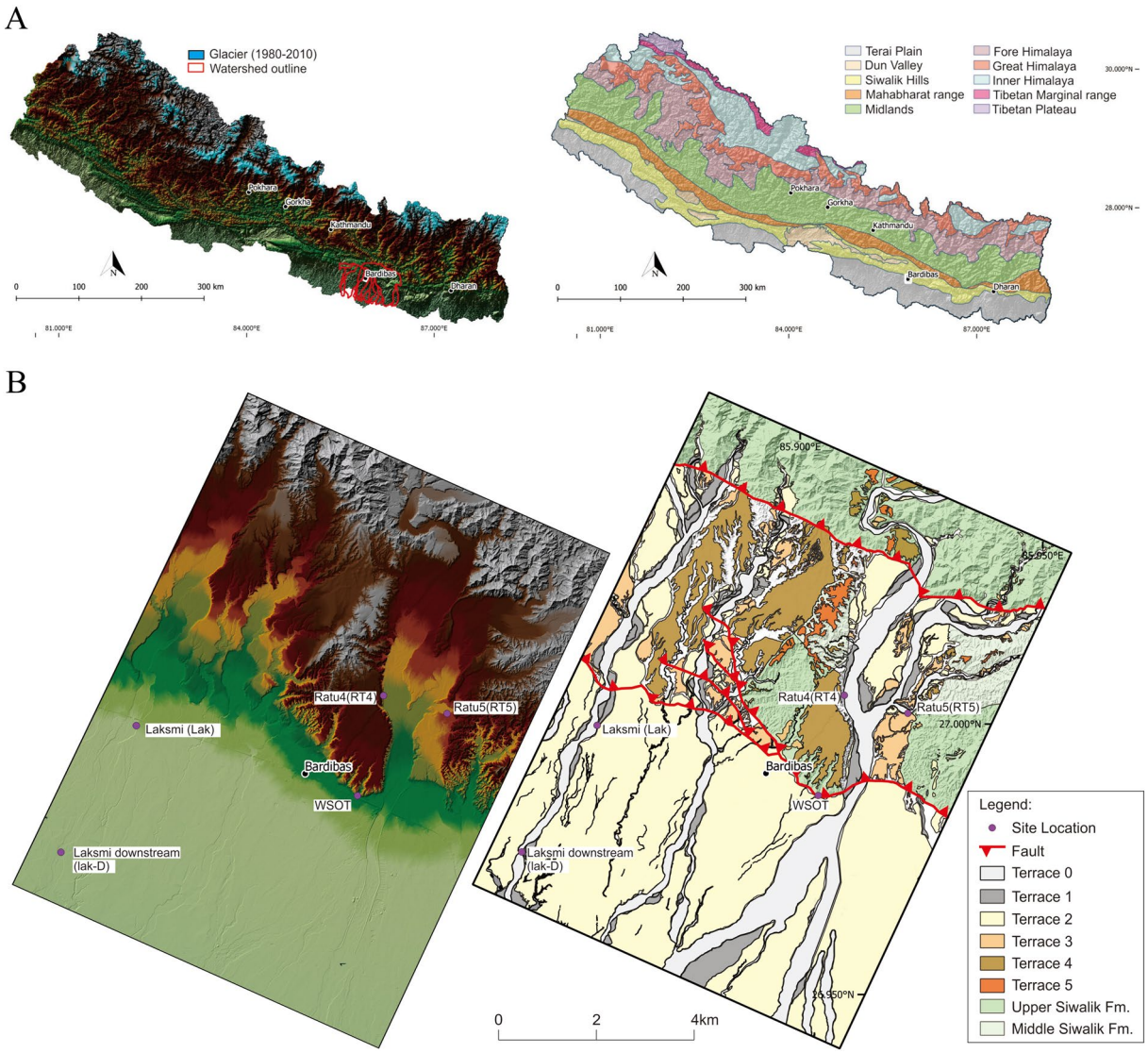

Fig. 1 **a** DEM, regional geology of the Himalayas (modified from Dhital 2015), Nepal. **b** Enlarged Lidar DEM with geomorphologic map of the area showing the Terai Plain and studied localities, loess and loess-like deposits sampling sites in the Bardibas region, central Nepal. Yellow areas of the Terai Plain (T2) are dominantly covered by loess and loess-like deposits

a mean annual rainfall at Jaleshwar and Tulsi meteorological stations of 1035 mm and 1609 mm, respectively (Khanal et al. 2007). The winter monsoon propagates south-eastwards from October to April, bringing winds from the NW and drier conditions than the summer monsoon.

The Lesser Himalayas are drained by small fluvial catchments that erode the continental clastic rocks of the Siwalik Group (Medlicott 1864; Gansser 1974; Delcaillau 1992; Dhital 2015). The aggradational Southern Terai Plain consists of Pleistocene to Holocene fluvial and alluvial fan deposits of coarse to fine-grained gravel, sandy and muddy deposits (Dhital 2015), and the aeolian deposits described here. The study area is cut across by the active Main Himalayan Frontal Thrust (Patu and Bardibas Thrusts) which tectonically uplifted Quaternary fluvial terraces along the rivers of the Himalayan piedmont zone (Bollinger et al. 2014, Almeida et al. 2018).

Materials and methods

This study involved fieldwork, geomorphologic mapping, sedimentological descriptions, and sampling, optically stimulated luminescence dating, grain size by laser diffraction, geochemical and mineralogical analyses by X-ray fluorescence (XRF) and X-ray diffraction (XRD), and SEM (scanning electron microscope). We present

selected results from five locations named Laksmi1, Laksmi downstream, RT4, RT5, and WSOT (Fig. 1). Sixteen samples were collected for grain-size analysis (Appendix 1). Satellite images and Digital Elevation Model (DEM) from the Shuttle Radar Topographic Mission (SRTM) at 90-m resolution were processed for geomorphologic mapping in Global Mapper and QGIS. A detailed 0.5-m high-resolution DEM was surveyed with Airborne Lidar by the Earth Observatory of Singapore from Khayarmara in the west to Puspalpu, with a coverage of 304 km^2. We processed both sources, LIDAR and SRTM in the Bardibas area, with an overlap coverage of 91.35 km^2 covering the study area.

Optically stimulated luminescence dating

Five loess and loess-like samples were dated for optically stimulated luminescence in the Luminescence Dating Laboratory at the Korea Basic Science Institute, using automated Risø TL/OSL measurement (Table 1). Quartz grains of 90–250 μm were prepared by wet sieving and acid treatments (10% HCl, 10% H_2O_2, and conc. HF). Equivalent doses were estimated using protocol SAR (Single-Aliquot Regenerative-Dose; Murray and Wintle 2000). For sample RT1-A which has higher Infrared Stimulated Luminescence of Feldspar (IRSL)/Blue light of Quartz signal ratios (>10%), a double-SAR procedure was carried out to determine their equivalent dose (De) values (Roberts 2007). All dose rates were modified using both present and saturated water contents and attenuation factors (Zimmerman 1971). Cosmic ray contributions were estimated after Prescott and Hutton (1994).

Table 1 Chemical Index of Alteration (CIA; Nesbit and Young 1982), Chemical Index of Weathering (CIW; Harnois 1988), Plagioclase Index of Alteration (PIA; Fedo et al. 1995), and Index of Compositional Variation (ICV; Cox et al. 1995)

Sample ID	CIA	CIW	PIA	ICV
WSOT	84.48	97.50	97.04	0.51
Lak2_D	73.69	85.80	83.01	0.80
Lak1_D	75.72	87.03	84.75	0.75
Lak2-3	76.67	88.32	86.23	0.70
RT4_SL3	78.87	94.96	93.67	0.70
RT4_U30	80.15	95.05	93.92	0.64
RT4_loess1	80.59	95.64	94.63	0.69
RT4_L3	79.79	95.50	94.40	0.65
Lak_02	77.93	90.62	88.80	0.71
RT5a2_SAS	80.88	95.73	94.77	0.66
RT5_1stS	80.02	95.51	94.43	0.64
RT5_MLS	79.39	95.11	93.90	0.63
Lak2-2	77.85	89.71	87.86	0.70
RT5_LUS	78.82	95.19	93.93	0.63
RT5a2_BS	79.50	95.48	94.35	0.61

Grain-size analysis

The grain-size distributions of sixteen samples were measured using a Malvern Mastersizer 3000 Hydro EV laser grain-sizer (Fig. 3). The distributions of the different particle sizes were quantified with GRADISTAT (Blott and Pye 2001).

Geochemistry

All samples were heated in an oven at 90 °C for 6 h to remove moisture, and crushed with a swing mill for XRF and XRD analyses. For XRF analysis, powdered samples were mixed with licowax binder to create stable pressed pellets. Major element analyses were carried out using an Energy-dispersive X-ray fluorescence (EDXRF) spectrometer S2 PUMA with the SPECTRA.ELEMENTS software.

Mineralogy

The XRD analyses were conducted using a D2 PHASER X-ray diffractometer, using CuKα radiation, an accelerating voltage of 30 kV, and a beam current of 10 mA. The scan range (2Θ) was from 1 to 70° with slit of 0.2 mm for 4 h. Minerals were identified qualitatively using phase identification by comparing the measured pattern of each crystalline phase with the Powder Diffraction File (PDF-2 2019) database. Qualitative and semi-quantitative analyses were carried out with the DIFFRAC.EVA software.

Scanning electron microscopy (SEM)

Eight loess and loess-like sediments have been studied under SEM to observe microtexture (Table 2). Preparation for grain morphology analyses involved 30% hydrogen peroxide (H_2O_2) and 10% hydrochloric acid (HCl). Samples were then washed with deionized water until the decanted water was clear. Grains were randomly selected under the binocular microscope and were placed on the stubs to get carbon coated. The Leica sputter coater EM ACE600 was used to produce very thin carbon layers. BE and SE images were obtained using JEOL SM-7800F Schottky Field Emission Scanning Electron Microscope. Twenty-five to thirty grains are observed per sample for this study of microtextures following the grain microtexture classification of Vos et al. (2014). The feature of surface grain micro-texture is called abundant when it is present on > 75% of the grains, common (50–75%), sparse (50–5%) and rare (< 5%).

Table 2 Microtextures of grain surfaces identified with SEM

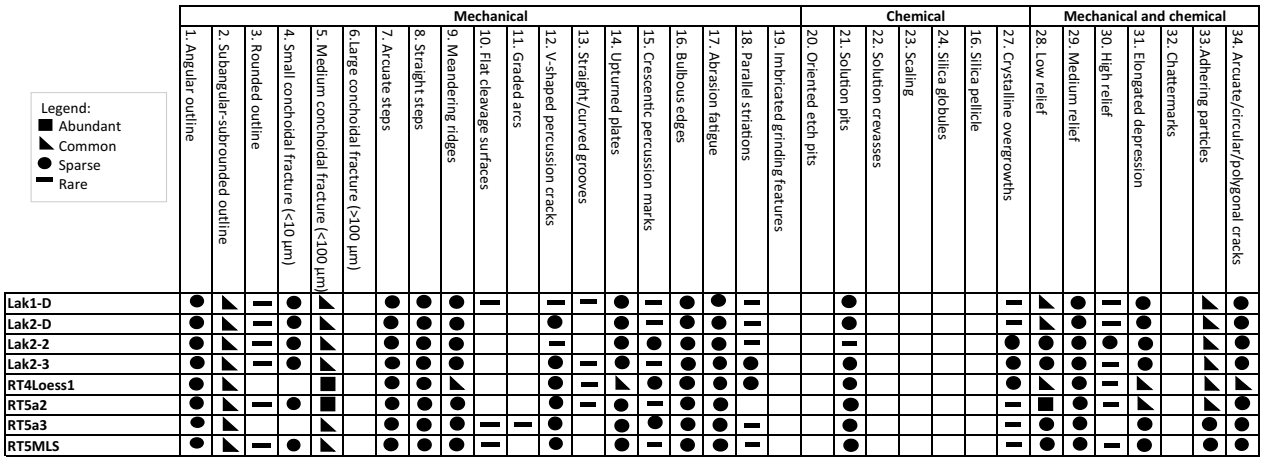

Results

While the deformation of the Himalayan Main Frontal Thrust (MFT) has been typically reconstructed by focusing on morphotectonics and the deformation of fluvial terraces, the presence of beds of Quaternary massive and friable yellowish silt-sized sediments in the Terai plain and fluvial terraces confirm the occurrence of loess, sandy loess, and sandy-silty fluvial–aeolian deposits. The Terai Plain is characterized by a flat silty surface and intense agricultural land use. We regionally identified four terrace levels in the pedemountain rivers, named from T1 (younger) to T4 (older), being the present river floodplains the level T0 (Figs. 1, 2). Previous studies included a fragmentary higher terrace in the MFT belt, bringing the total to five levels (Bollinger et al. 2014). The aeolian deposits, the focus of this article, were identified in river banks outcrops, correlated with Terraces 2 and 1, and on the regional surface of the Terai Plain. They are typical loess and sandy loess deposits, a clastic loose silty sediment with unstratified structure, porous, permeable, erodible, brown in color and with vertical banks.

Loess and related aeolian deposits

The composed Laksmi section is located on the Lakshmi River's bank and exposes terraces T1 and T2 (Figs. 1, 2). Sample Lak 1–1, a silty fine sand from T2, yields an age of 4.8 ± 0.3 ka. The youngest OSL dating sample of a loess (fine sandy-silt sediment) from Laksmi's section, Lak 2–1 (1.0 ± 0.1 ka), was collected from T1. The total thickness of the aeolian deposits in Lakshmi section (Fig. 2) reach 1.6 m of very fine sandy coarse silt loess (Lak 2.2).The correlative Lakshmi downstream section is composed also of ~ 1.7 m of loess (samples Lak 1-D with 51% silt, Lak 2-D with 64% silt, Fig. 3 and Appendix A.1).

In the Laksmi Downstream profile (T1), Sample Lak 1-D has a unimodal size of 67 µm with 61% of silt-sized particles. Sample Lak 2-D has a unimodal size of 94 µm with 51% of silt-sized particles. Both samples Lak 1-D and Lak 2-D are defined as coarse primary loess according to Vandenberghe (2013), Vandenberghe et al. (2018) (Fig. 3, Appendix A.1), whereas Lak 2–3 show bimodality of 1 µm and 24 µm. They have 75% and 72% silt-sized particles, respectively.

In Ratu tributary, section RT 5 is from T2, with OSL ages of 5.8 ± 0.6 (RT1) for loessic fine sandy silt, 4.0 ± 0.2 (RT1-A) for very fine sand, and 2.6 ± 0.3 ka (RT2) for a primary loess with 62% of silt, (RT5a2-SAS) from the lower, middle and upper parts of the section, respectively (Fig. 2). In Ratu RT5 profile (T3), samples RT5 1st, RT 5 MLS, and RT5 LUS show unimodal grain-size distributions, with a modal size of more than 134 µm. They are fine to very fine sands, with 12–29% of silt-sized particles. Sample RT5a-2 SAS from RT5 profile shows polymodal sizes of 7.5 µm, 67 µm, and 267 µm with 62% of silt-sized particles.

In RT4 profile (T2), samples RT4 Loess1 and RT4 SL3 show unimodal size distribution ranging from 119 µm and 106 µm, respectively, with less than 50% silt-size particles. Sample RT4u30 from RT4 profile indicates trimodal sizes of 1 µm, 7 µm, and 150 µm with 55% of silt-sized particles. These sediments fall into the coarsest loess sediment group.

Importantly, widespread loess is blanketing the T2 surface that regionally dominates the Terai Plain (Fig. 1). The sample WSOT from that surface shows a primary loess population with a unimodal size of 53 µm, and 72% of silt-sized particles, and a modal grain size in the medium- to coarse-grained silt fraction. It is relevant because demonstrates that loess is even purer on the plain and becomes

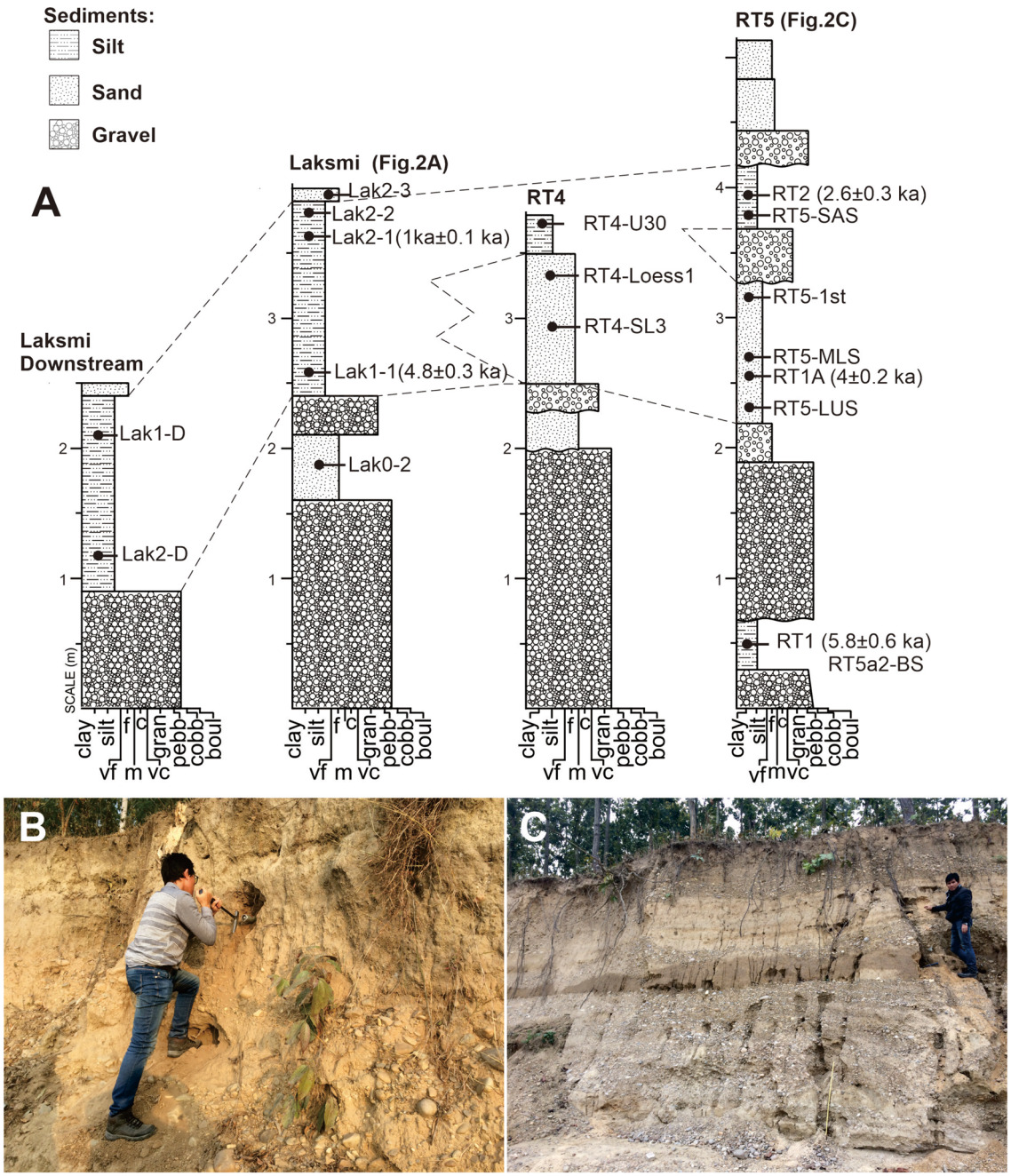

Fig. 2 **a** Stratigraphic sections of the river terraces with OSL ages. Photographs of Loess deposits covering fluvial deposits in **b** Laksmi downstream, and **c** Ratu 5 site

sandier when deposited closer to the fluvial belts. It has to be considered that sandy loess are derived from some proximal fine sand source such as fluvial deposits, sand dunes, coastal areas, piedmont areas, glaci-fluvial deposits, among others, and were recorded worldwide (Pye 1995; Ding et al. 1999; Zárate 2003; Scull and Schaetzl 2011; Vandenberghe 2013; Li et al. 2017; Costantini et al. 2018; among others). The presence of sandy loess close to the fluvial belts of the Terui Plain is a consequence of fluvial aeolian interactions in the Himalayas piedmont where loess deposition is widespread, but the additional source of fine sands from the fluvial systems occurs

Similarly to typical loess from other regions of the planet, the Bardibas loess and loess-like sediments

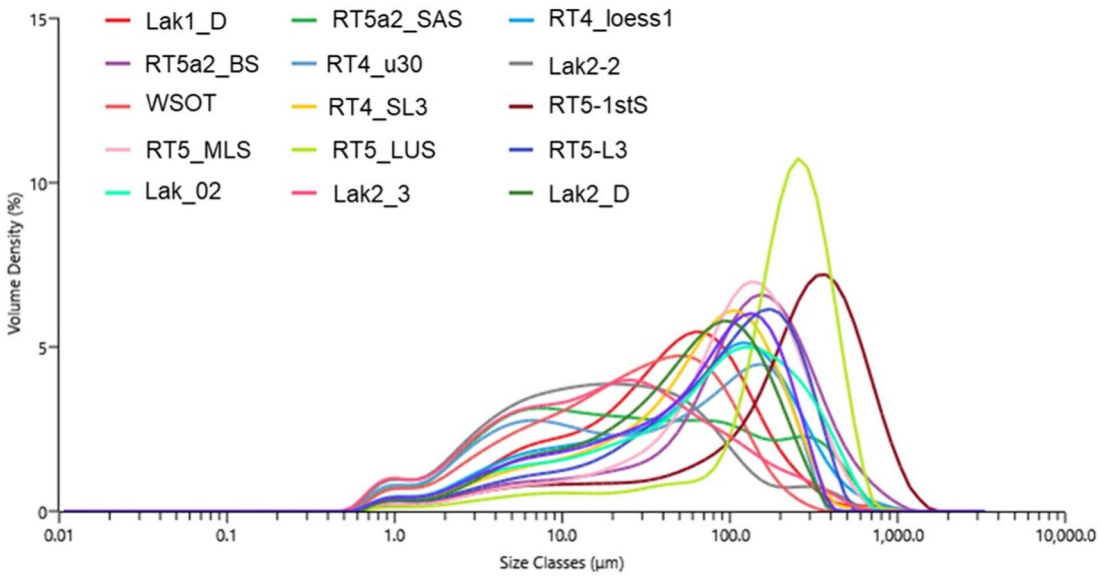

Fig. 3 Grain-size distribution curves of loess and loess-like in Bardibas

are rich in SiO_2, which ranges from 78.37% to 93.84% (Appendix A.2). Al_2O_3 ranges from 5.09% to 12.3%, Fe_2O_3 ranges from 0.95 to 3.94%, K_2O ranges from 0.75% to 1.95%, and MgO ranges from 0.34% to 1.67%. Na_2O, CaO, TiO_2, and P_2O_5 are present only in minor (< 1%) amounts.

The XRD analyses on bulk samples of loess indicate that quartz, mica (muscovite and illite), and potassium feldspar (microcline, orthoclase, and sanidine) are the dominant minerals, comprising more than 90% of the total (Appendix A.3.). The remaining minerals include kaolinite, plagioclase (albite), and carbonate minerals (calcite, dolomite, and aragonite). The average mineralogical composition is 84.7% quartz, 5.4% potassium feldspar, 7.4% mica, 0.37% kaolinite, 0.9% plagioclase, and 0.22% carbonate minerals.

Discussion

Grain-size analysis concerning provenance

Based on the grain-size analysis, the aeolian deposits consist of primary loess, sandy loess, and to a minor degree local secondary loess (sandwiched loess beds in between alluvial beds).

Loess sediment with a modal grain size in the fine-sand modal fraction is possibly derived from a local sandy source between several hundred meters to a few kilometers away (Enzel et al. 2010; Vandenberghe 2013). However, loess particles in the medium- to coarse-grained silt modal fraction could have been transported across tens of kilometers (Vandenberghe 2013). Thus, primary loess covers the Terai Plain where the silt fraction can reach up to 72%. Dust particles transported across larger distances are characterized by the fine-silt and clay fraction (between 4 µm and 22 µm) (Fig. 3). This finer loess modal fraction is recorded only as a sub-population in secondary loess (reworked or mixed, loess-derived sediment). These polymodal grain-size distributions indicate an imprint of long-distance deposition of loess affected by (secondary) post-depositional processes of local sandy supply (fluvial and aeolian) and reworking by rivers or surface runoff (Vandenberghe 2013; Vandenberghe et al. 2018). It suggests that sediment is likely to experience cycling episodic transportation and deposition prior to dominant entrainment and deflation by wind.

At least one billion tons of siliciclastic detritus are currently produced annually by erosion of the active Himalayan range from 380×10^6 ty^{-1} to 480×10^6 ty^{-1} (Lupker et al. 2012; Lupker et al. 2013; Borromeo et al. 2019). The area has been sourced and acted as a trapping zone of fluvial sediments since the Pleistocene when large megafans developed in the area, and the Kosi megafans are still active. The vast Kosi and Gandak megafans (Mohindra and Parkash 1994; Sinha et al. 2014), and particularly the vast alluvial interfans area of the Tepui plain are possibly the main proximal sources of the Holocene loess in our study area.

Furthermore, fine-grained sediments (clay and perhaps silts) deposited during the Holocene in the Ganga Basin along the Ganga river system to the Bay of Bengal are also a possible secondary source for the silt and clay fraction although further analyses are required to confirm it.

Mineralogy, major element content, and SEM, regarding weathering and provenance

Beyond local–regional sources, there are other potential sources to be considered for the loess in our study, from the furthest to closest: Chinese Loess Plateau, Kashmir Valley, and, as discussed above, the Himalayan foreland fluvial systems of the Ganges River Basin. To interpret provenance and its weathering effect, we carried out bulk mineralogy and chemical analyses.

For comparison, we plotted the concentrations of the major elements that represent clay, carbonates, feldspars, and micas from the Chinese Loess Plateau, Kashmir Valley, and this study loess deposits. Loess in the study area contains less abundant clay minerals (Fig. 4a) and lacks a significant amount of carbonate minerals (Fig. 4b), and fewer feldspars and micas than in the other potential source regions (Fig. 4c). The predominant quartz and SiO_2 content in the Bardibas samples indicates quartz-rich source rocks (Fig. 4b; Appendix A.3). The loess and loess-like deposits of our study are clustered differently than other characteristic loessic areas, indicating specific characteristics and different regional sources.

The lack of correlation with distant sources indicates that the most probable are regional source areas of the lesser Himalayas and foothills areas where the Siwalik rocks and derived Quaternary alluvial proximal piedmont deposits are widespread. Thus, we compared the mineralogy of the Siwaliks rocks with the bulk mineralogy composition of loess and loess-like sediments in Bardibas.

Petrographically, the Siwaliks sedimentary rocks are predominantly quartzolithic and include monocrystalline to fine-grained polycrystalline quartz, followed by potassium feldspar, plagioclase, and common to rare lithic fragments comprised gneiss, schist, limestone, dolomite, chert, shale, crystalline quartzite, and volcanic rocks (Ranjan and Banerjee 2009; Tamrakar and Syangbo 2014). Muscovite and biotite are scarce in the Lower Siwaliks but increase toward the Upper Siwaliks (Tokuoka et al. 1988; Tamrakar and Syangbo 2014). The Siwaliks mudstone is composed of illite, chlorite, smectite, sepiolite, and mixed clays (Chaudhri and Gill 1983; Raiverman and Suresh 1997; Suresh et al. 2004).

The ternary plot of bulk clay minerals suggests a low kaolinite/ilite ratio. Indicates dominant physical erosion and weak chemical weathering (Fig. 5a; e.g., Liu et al. 2007, Liu et al. 2012; Chen et al. 2017; Sang et al. 2018). Potassium feldspar is found as the main component in the Siwaliks rocks and the Bardibas loess and loess-like sediments. Muscovite is probably derived from the middle and upper parts of the Siwaliks rocks and/or from the physical erosion of metamorphic lithic fragments. Illite may have been formed by weathering of potassium feldspar under moderate hydrolysis conditions, degradation of mica, and/or physical erosion of metamorphic and granitic lithic fragments (Chamley 1989; Thiry 2000; Liu et al. 2007).

Bulk geochemical analyses were carried out to examine chemical signatures of the source terrain of loess and loess-like deposits. The geochemical signature provides information on the complex geologic interaction of several variables such as source terrain composition, weathering environment, transport, and diagenesis (McLennan 1993).

Grain size correlates with the Al_2O_3 and SiO_2, which Al_2O_3 increases in finer sediments (primary loess silt) and SiO_2 with sand content (Fig. 6). SiO_2 shows a negative correlation with Al_2O_3 ($R^2=0.98$) and TiO_2 ($R^2=0.92$) suggesting that SiO_2 is mainly present as quartz grains. A strong positive correlation of TiO_2 with Al_2O_3 ($R^2=0.93$),

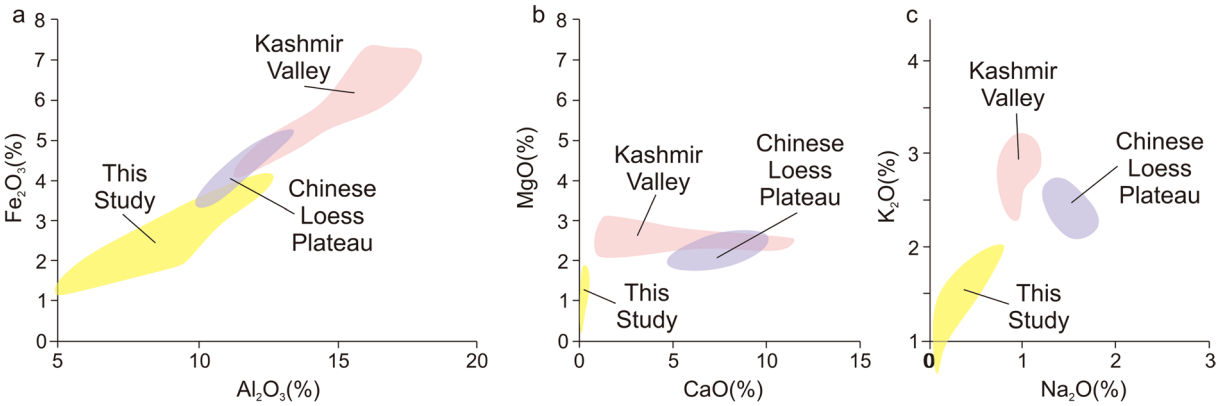

Fig. 4 Plots of major elements concentrations indicatives of **a** clay minerals, **b** carbonate minerals, and **c** feldspars and micas from loess deposits in Chinese Loess Plateau, Kashmir Valley and this study. Data sources for the Chinese Loess Plateau from Muhs (2018) and Kashmir Valley from Ahmad and Chandra (2013)

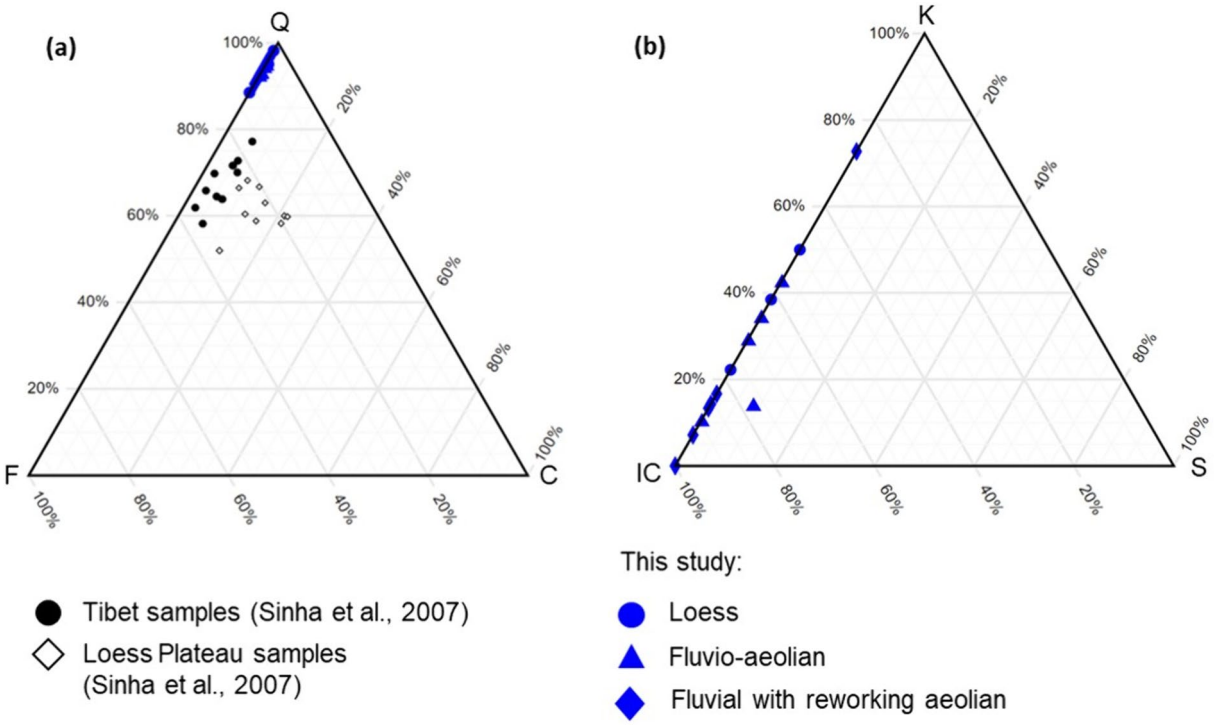

Fig. 5 **a** Ternary diagram comparing the relative abundance of Quartz–Feldspar–Calcite (Q–F–C) between the loess and loess-like deposits from Tibet, Loess Plateau (from Sun et al. 2007), and this study, and **b** clay minerals of kaolinite–illite + chlorite–smectite (K–IC–S) in loess and loess-like deposits from Bardibas

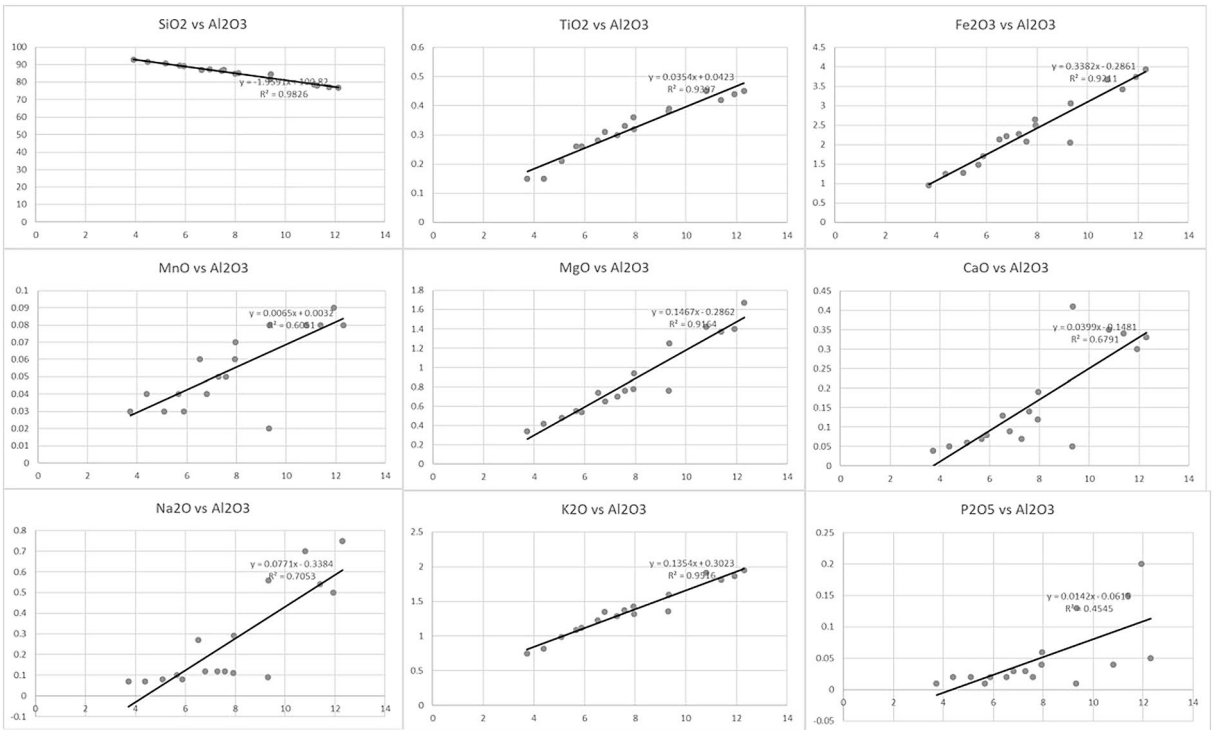

Fig. 6 Scatter plots of Bardibas loess and loess-like deposits major oxides and Al_2O_3 percentage

Fe_2O_3 ($R^2=0.92$), and MnO ($R^2=0.6$) indicates the occurrence of TiO_2 in the clays. A positive correlation of CaO to TiO_2 ($R^2=0.67$) and Al_2O_3 ($R^2=0.67$) suggests the presence of carbonate minerals. The Al_2O_3 correlates positively with K_2O ($R^2=0.95$), Na_2O ($R^2=0.7$), and MgO ($R^2=0.91$) suggesting that the concentrations of the K-bearing minerals have a significant influence on aluminum distribution (McLennan et al. 1983; Jin et al. 2006; Babeesh et al. 2017). A lower ratio of K_2O/Al_2O_3 indicates a predominance of clay minerals over K-bearing minerals (Cox et al. 1995; Ahmad and Chandra 2013). The calculated Index of compositional variation for all samples shows values < 1 (from 0.5 to 0.79, average 0.67) pointing to clay minerals such as kaolinite, illite, and muscovite (Cox et al. 1995; Moosavirad et al. 2011; Babeesh et al. 2017).

Constraining at the regional al scale, we compared our results with the Fe/Si, Na/Si, and K/Si ratios and the Al/Si ratio from the river sediments covering the Ganga basin rocks (Fig. 7a–c; Lupker et al. 2012). All elements, except Na, show a systematic positive correlation with Al/Si. This positive correlation suggests the concentration of Fe-bearing (e.g., biotite, sheet silicate iron clay, and Fe-hydrox.) and K-bearing minerals (such as illite and muscovite). The K and Na ratio indicates the relative abundance of potassium feldspar to plagioclase.

The chemical compositions of the loess and like-loess sediments also were compared to the Neogene Siwalik rocks by plotting the molar proportions of Al_2O_3, CaO^*+Na_2O, K_2O (A-CN-K) and Al_2O_3, $CaO^*+Na_2O+K_2O$, $FeO+MgO$ (A-CNK-FM), where CaO^* represents Ca in silicate-bearing minerals only (Nesbitt and Young 1982). The bulk composition plots on the A-CN-K and A-CNK-FM diagrams show that all fall onto one cluster (Fig. 8). A tendency of aeolian samples distribution to the left from the Siwaliks rocks (Fig. 8) suggests progressive processes of weathering, as the bulk composition evolves toward the A-K line. CaO^*+Na_2O is removed in preference to K_2O. It results in a trend that is subparallel to the left boundary, which suggests that Ca and Na are taken up by illite and muscovite (Fig. 8).

The geochemical results point out that the Siwaliks rocks are the most plausible parent rocks for Bardibas loess and loess-like deposits.

We additionally estimated the degree of weathering by applying the Chemical Index of Alteration (CIA; Nesbitt and Young 1982) and Chemical Index of Weathering (CIW; Harnois 1988) (Table 3). CIA values range from 73 to 84 (average 78; Appendix A.2) similar to the CIA value of the Neogene Siwalik mudstones (average 75; Sinha et al. 2007) and sandstones (average 79; Ranjan and Banerjee 2009). The CIW value ranges from 84.8 to 97.5 (average 92, Appendix A.2) and is comparable to the Siwalik mudstones (average 88; Sinha et al. 2007) and sandstones (average 90; Ranjan and Banerjee 2009). Insignificant changes in CIA and CIW values suggest recycling or re-sedimentation of the possible Siwalik source into the Terai Plain without notable chemical weathering. The presence of clay minerals such as illite, muscovite, and kaolinite is characterized by a low value of the index of compositional variation (ICV from 0.5 to 0.79, average 0.67; Cox et al. 1995; Moosavirad et al. 2011; Babeesh et al. 2017).

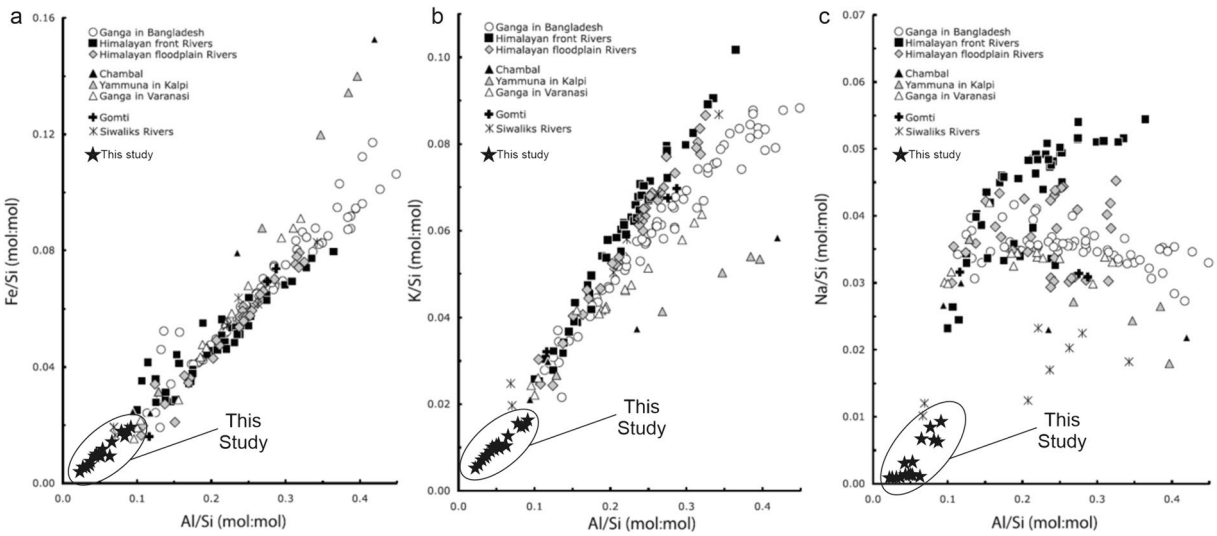

Fig. 7 **a** Fe/Si, **b** K/Si, and **c** Na/Si ratios of the main Ganga rivers system and this study. The chemical compositions of the Ganga River system are from Lupker et al. (2012)

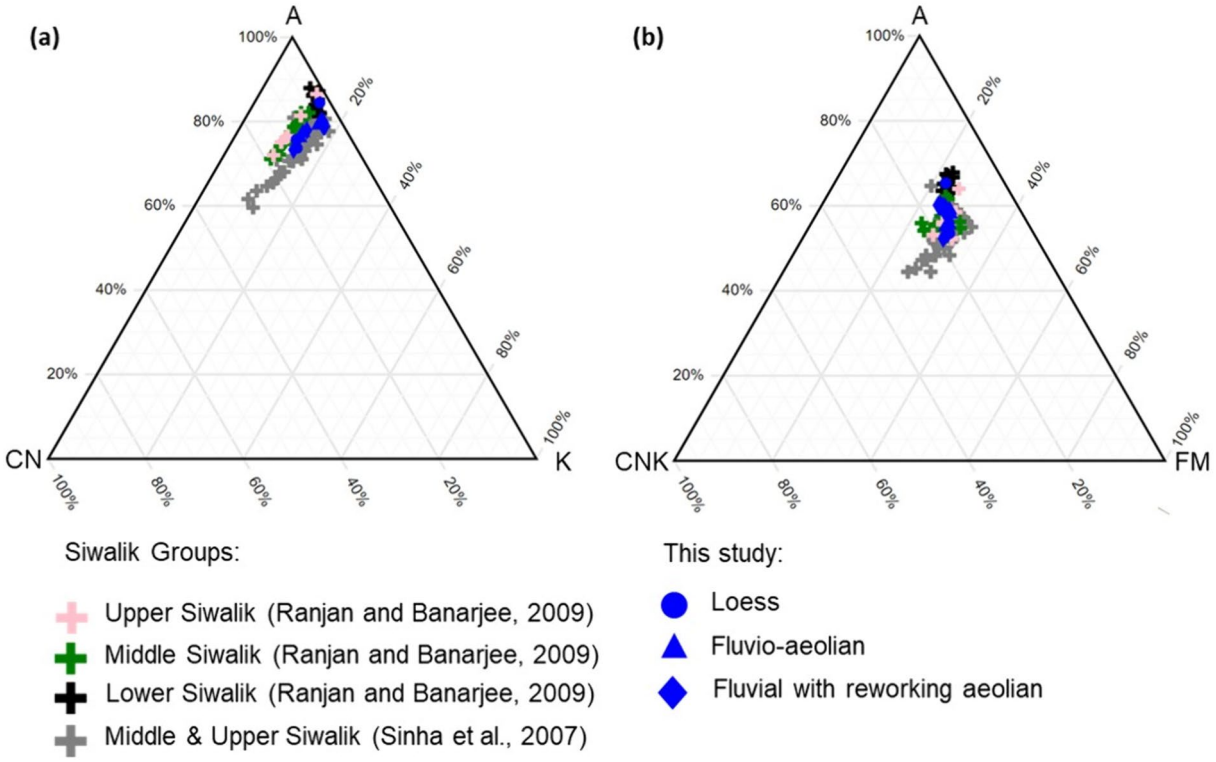

Fig. 8 **a** Ternary plots comparing relative abundances of AL_2O_3–CaO* + Na_2O–K_2O (A-CN-K) and **b** Al_2O_3–CaO* + Na_2O + K_2O–FeO + MgO (A-CNK-FM) between Siwalik sediments (from Sinha et al. 2007; Ranjan and Banerjee 2009) and loess and loess-like deposits in this study

Table 3 OSL dating

Sample	Dose rate (Gy/ka)*	Water content[a] (%) present (saturated)	Equivalent dose (Gy)	Aliquots used[b] (n/N)	OSL age[a,c] (ka, 1σ SE)
RT1	1.24 ± 0.04 (0.93 ± 0.03)	0.2 (29.9)	7.2 ± 0.7	16/16	5.8 ± 0.6 (7.7 ± 0.7)
RT2	2.13 ± 0.06 (1.60 ± 0.04)	0.3 (31.3)	5.6 ± 0.5	16/16	2.6 ± 0.3 (3.5 ± 0.3)
RT1-A	1.91 ± 0.05 (1.46 ± 0.04)	0.2 (29.1)	7.6 ± 0.4	16/16	4.0 ± 0.2 (5.2 ± 0.3)
LAK1-1	2.60 ± 0.07 (1.97 ± 0.05)	0.6 (29.5)	12.4 ± 0.7	16/16	4.8 ± 0.3 (6.3 ± 0.4)
LAK2-1	3.59 ± 0.08 (2.64 ± 0.06)	2.0 (35.0)	3.6 ± 0.2	16/16	1.0 ± 0.1 (1.4 ± 0.1)

[a] Numbers in parentheses are those calculated based on saturated water contents

[b] *n/N* refers to the ratio of (the number of aliquots used for data analysis)/(total number of aliquots used for OSL measurement)

[c] Central age ± 1σ standard error

In conclusion, the mineralogical and geochemical of the loess and like loess deposits and the regional geochemical and mineralogical data from the Siwalik sediments (Chaudhri and Gill 1983; Tokuoka et al. 1988; Raiverman and Suresh 1997; Suresh et al. 2004; Ranjan and Banerjee 2009; Tamrakar and Syangbo 2014) points the Siwalik Group as the most plausible parental rocks.

SEM—scanning electron microscope

In terms of loess genesis, there is still considerable debate about the specific processes whereby silt particles are generated before they are entrained by the wind (Muhs 2018). To address this issue we identified microtextures on grain surfaces using SEM (Table 2). Grain surface microstructures and morphology provide an insight into the sedimentary history and cycle of clastic sediments in different depositional environments (Velbel 2007; Vos et al. 2014).

In accordance with the geochemical result, grains of the loess and loess-like deposits are dominated by quartz grains that are typically sub-angular to sub-rounded, indicating that the edges and corners had been eroded

by particle collisions during long transport or multicycle processes. Collision pits, such as dish-like and crescent-like depressions are usually formed as a result of high-speed impact among well-rounded particles and are the most typical features of quartz grain in aeolian sediment (Fig. 9a, Chen et al. 1986; Wang et al. 2018, 2019). In addition, upturned plate cleavage was also observed (Fig. 9b). Chemical weathering is indicated by pits, grooves, and holes on the grain surfaces (Fig. 9d).

Loess and loess-like sediments chronology

The OSL ages are evidence that the Bardibas primary loess began to deposit at ca. 4.8 ka, and continued accumulating up to ca. 1 ka (Table 1). The age range correlates with the last recorded phase of loess deposition in intra-mountains basins of the Central Himalayas in the India territory (Pant 1993), ~ 700 km to the ENE of our study area, and the record of near 40 cm of loess deposition at ca. 2.5 ka in southern Zanskar range, northwestern Himalaya, approximately 1200km far away from our study area (Lone et al. 2023). The chronology is also correlative with dune building in the Thar Desert between 4.5 ka and 3.1 ka (Thomas et al. 1999). Additionally, the chronology is supported by a sharp drop in temperature and rainfall recorded around 4 ka in the Central Himalayas (Phadtare 2000). It overlaps with the decrease in precipitation from ~ 4 ky–3 ka linked to the deterioration and collapse of the Harappan/ Indus civilization and Ghaggar culture in northern India and the decrease in precipitation recorded in speleothems records (Kotlia et al. 2015; Leipe et al. 2014; Tripathi et al. 2004). Regarding loess records in Nepal, a couple of meters to less than a meter of loess ca. 3.0–4.0 ka were described along the Imja Drangka valley, in the Khumbu Himal high mountains, with thickness decreasing with elevation (Baumler 2001).

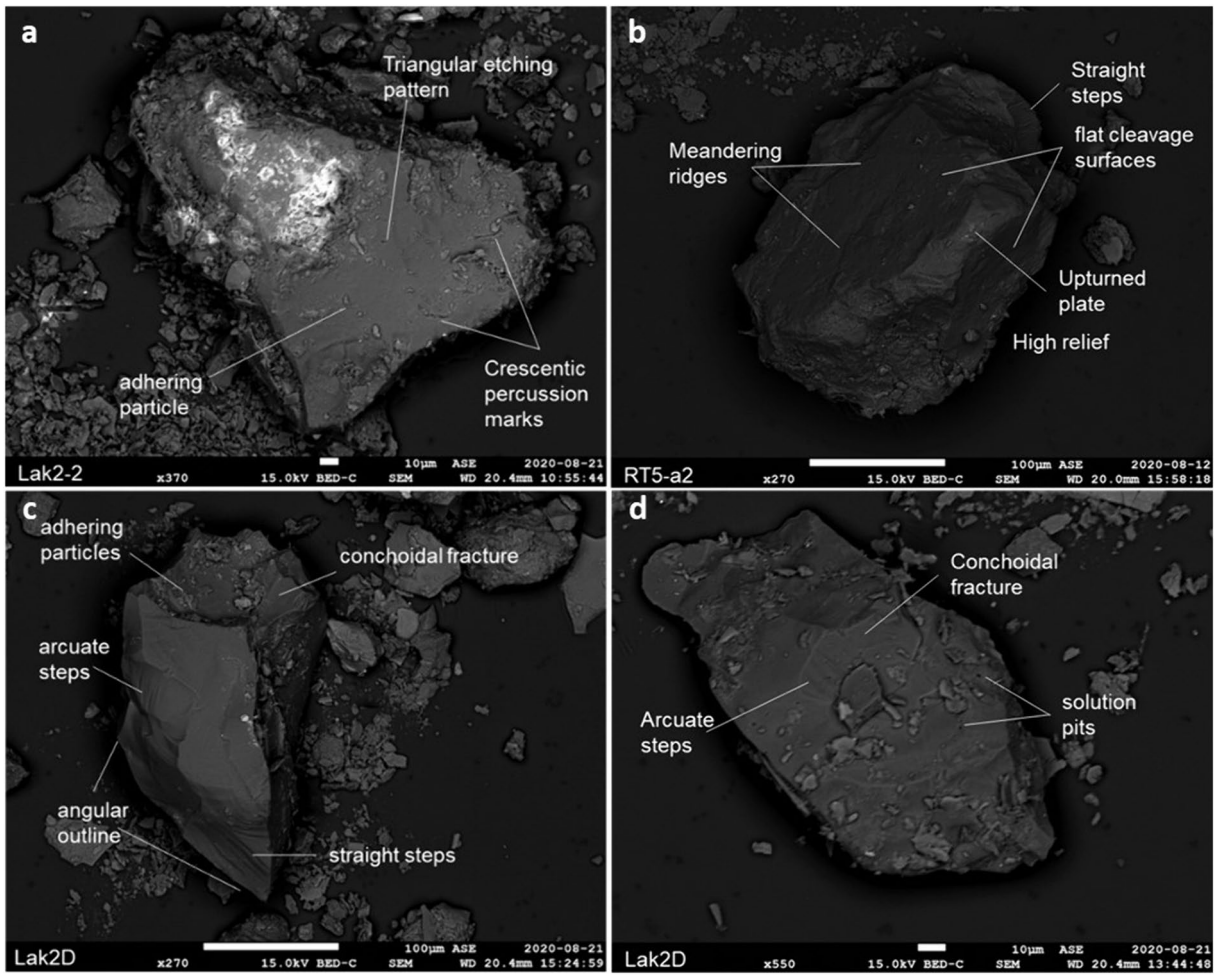

Fig. 9 SEM images showing **a** Sample Lak2-2: crescentic percussion marks, triangular etching pattern, and adhering particles. **B** Sample RT5-a2: (**b**) upturned plate, flat cleavage surface, straight steps and meandering ridges. **c** And (**d**) sample Lak2D: conchoidal fracture, arcuate and straight steps, adhering particles and solution pits

Despite the long distances and the orographic barrier represented by the Himalayas, there are potential correlations between the proxy records from the northern flank of the Himalayas and the Tibetan Plateau. Drought events correlate with loess units at ca. 5.8–6.8 ka in eastern Tibet (Lehmkuhl et al. 2014), while fluvial–eolian loess deposition at ca. 2.6 ka is synchronous with several lake and peat records from southeastern Tibet, pointing to a shift to a cold-dry climate at ca 3 ka to 2.5 ka (Shen 2003; Shen et al. 2006; Zhou et al. 2010). In the northeastern Tibetan Plateau, sand dunes have also been reactivated between 3 ka and the present (Stauch et al. 2012). A drier climate in the late Holocene is also well documented in many other records in monsoonal China and central Asia, and it is interpreted as a result of a decrease in monsoon intensity (An et al. 2000; Herzschuh et al. 2006; Zhao et al. 2009; Zhao and Yu 2012; Zhang et al. 2015). A decreasing energy of solar insolation in the area has been proposed (20°N to 35°N) from 5 to 1 ka (Yuan et al. 2004; Bird et al. 2014; Ramisch et al. 2016; Wang et al. 2019; Huang et al. 2020; Banerji et al. 2020) which might be related to monsoon weakening. In addition, Rashid et al. (2007) also reported a weak Indian Summer Monsoon phase after 5.5 ka in the Andaman Sea, and a significant weakening of ISM was also reported in North and northeast India (28°N to 36°N) ~ 4 ka (Berkelhammer et al. 2012; Bhushan et al. 2018; Banerji et al. 2020). The records reviewed above suggest phases of weakened summer monsoon with a drier and dustier climate in Southern Asia and Tibet during the late Holocene.

Currently and locally, dust storms commonly take place in Nepal during winters, with the Himalayas acting as a barrier to winds, and deflecting wind direction. Thus, we caution against a simplistic correlation of loess or other paleoenvironmental climatic proxy records on both flanks of the Himalayas. For example, the Nepal loess from this study has significantly higher amounts of quartz and lower amounts of calcite compared to loess samples from other regions in Asia (Fig. 4), which points to different provenances of the Bardibas loess and the Tibet and the Chinese Loess Plateau.

We suggest that the winter monsoon played a major role in the deposition of loess between 4.8 ka and 1 ka. Currently, the wind system is best developed during the dry season, which is typically October through May, with localized and strong mountain–valley wind circulations (Ramage 1971; Ohata et al. 1981). In comparison, winds are quite weak, with gusts at their minimum strength, particularly in August during the summer monsoon (Tartari et al. 1998). Although the data on the present winds patterns in the Lesser Himalayas foothills are scarce, near-surface winds blow mainly from the northwest (N330°E) to the east and northeast (N30°E–N110°E) (https://earth.nullschool.net). The average wind speed is less than 4 m/s during winter high-wind system and secondary local circulation piedmont winds (Laudari et al. 2018; https://earth.nullschool.net).

Final remarks

This study reports the first record of loess and loess-like deposition in eastern Nepal and presents integrated results of sedimentology, geochemistry, geochronology, mineralogy, and SEM. The late Holocene (4.8–1 ka) loess and related deposits in the Bardibas region were dominantly sourced locally from deflation Quaternary sediments of the Terai Plain which spread on the Kosi Gandak interfan area. The mineralogy, geochemistry, and SEM data of loess and loess-like deposits from the Bardibas area of the Terai plains indicate that these were derived from moderately weathered regional sedimentary source regions, and were subjected to a very low degree of chemical weathering after deposition. The high tectonic instability in the source area and geomorphology with cycles of aggradation and degradation by the fluvial systems in the Himalayas foothills did not favor intense and long-term chemical weathering of piedmont deposits. The mineralogical and geochemical compositions of the loess and loess-like deposits are related to those of the Siwalik rocks and those re-transported materials from rivers draining the Lesser Himalayas. The late Holocene loess and loess-like sediments in the Himalayan piedmont of Nepal were deposited during periods of weak activity of the Indian Summer Monsoon. Once entrained, this material would have been regionally carried in easterly and north-easterly directions, with the coarser material being deposited closer to the source area while the very fine material was carried out of the system in a long range of suspension. Specifically at the study area, the Terai alluvial plain sediments, sourced by fluvial catchments eroding the Siwalik Group in the Lesser Himalayas, were reworked by surface winds, probably with a northeast- and eastwards direction, during the winter monsoon. The role of the summer monsoon and the limited remote sources of fine dust can also be considered, but this needs further analysis. The chronologies of the loess and aeolian-related deposits in the Bardibas area correlate with thin intermountain loess deposits from the Central Himalayas in India.

Supplementary Information

The online version contains supplementary material available at https://doi.org/10.1186/s40562-024-00338-6.

Supplementary Material 1: Appendix A.1. Grain size statistics of loess and loess-like deposits in Bardibas area. **Appendix A.2.** Major oxides of

loess and loess-like deposits in Bardibas area. **Appendix A.3.** Major mineralogy of loess and loess-like deposits in Bardibas area.

Acknowledgements
The authors want to thank R. Almeida, M. Hamahashi, and L. Thu for their collaboration during fieldwork surveys, J. Hubbard for helpful discussions, and P. Adamek for his assistance with the manuscript style. We acknowledge Jeong-Heon Choi and Hou Ran for their OSL and XRF contributions.

Author contributions
Edgardo M. Latrubesse (EML) conducted fieldwork in Nepal, discovered the loess deposits, collected the samples for sedimentology, mineralogy, and OSL, and analyzed and mapped the geomorphology and stratigraphy of the region. Abang Nugraha (AN) conducted Remote sensing processing of SRTM and LIDAR, the XRD-XRF, grain-size analyses, and SEM, and prepared the figures. Both authors participated in the preparation of the manuscript, discussions, and interpretation of the data.

Funding
This study was supported by the National Research Foundation Singapore under its Singapore NRF Fellowship scheme (National Research Fellow Award No. NRF-NRFF2013-06), and by the EOS and the National Research Foundation Singapore and the Singapore Ministry of Education under the Research Centres of Excellence initiative.

Availability of data and materials
Additional lab data are provided in a supplementary file.

Declarations

Competing interests
The authors declare that they have no known competing financial interests or personal relationships that could have appeared to influence the work reported in this paper.

Received: 16 September 2022 Accepted: 20 April 2024
Published online: 23 May 2024

References

Ahmad I, Chandra R (2013) Geochemistry of loess-paleosol sediments of Kashmir Valley, India: provenance and weathering. J Asian Earth Sci 66:73–89. https://doi.org/10.1016/j.jseaes.2012.12.029
Almeida RV, Hubbard J, Liberty L, Foster A, Sapkota SN (2018) Seismic imaging of the main frontal thrust in Nepal reveals a shallow décollement and blind thrusting. Earth Planet Sci Lett 494:216–225. https://doi.org/10.1016/j.epsl.2018.04.045
An Z, Porter SC, Kutzbach JE, Xihao W, Suming W, Xiaodong L, Xiaoqiang L, Weijian Z (2000) Asynchronous Holocene optimum of the East Asian monsoon. Quat Sci Rev 19:743–762. https://doi.org/10.1016/S0277-3791(99)00031-1
Babeesh C, Achyuthan H, Jaiswal MK, Lone A (2017) Late Quaternary loess-like paleosols and pedocomplexes, geochemistry, provenance, and source area weathering, Manasbal, Kashmir Valley, India. Geomorphology 284:191–205. https://doi.org/10.1016/j.geomorph.2017.01.004
Banerji US, Arulbalaji P, Padmalal D (2020) Holocene climate variability and Indian Summer Monsoon: an overview. The Holocene 30(5):744–773
Bäumler R (2001) Pedogenic studies in aeolian deposits in the high mountain area of eastern Nepal. Quat Int 76–77:93–102. https://doi.org/10.1016/S1040-6182(00)00093-8
Berkelhammer M, Sinha A, Stott L, Cheng H, Pausata FS, Yoshimura K (2012) An abrupt shift in the Indian monsoon 4000 years ago. Geophys Monogr Ser 198:75–87
Bhushan R, Sati SP, Rana N, Shukla AD, Mazumdar AS, Juyal N (2018) High-resolution millennial and centennial scale Holocene monsoon variability in the Higher Central Himalayas. Palaeogeogr Palaeoclimatol Palaeoecol 489:95–104
Bird BW, Polisar PJ, Lei Y, Thompson LG, Yao T, Finney BP, Bain DJ, Pompeani DP, Steinman BA (2014) A Tibetan lake sediment record of Holocene Indian summer monsoon variability. Earth Planet Sci Lett 399:92–102
Blott SJ, Pye K (2001) Gradistat: a grain size distribution and statistics package for the analysis of unconsolidated sediments. Earth Surf Process Landforms 26:1237–1248. https://doi.org/10.1002/esp.261
Bollinger L, Sapkota SN, Tapponnier P, Klinger Y, Rizza M, Van Der Woerd J, Tiwari DR, Pandey R, Bitri A, Bes De Berc S (2014) Estimating the return times of great Himalayan earthquakes in eastern Nepal: evidence from the Patu and Bardibas strands of the Main Frontal Thrust. J Geophys Res Solid Earth 119:7123–7163. https://doi.org/10.1002/2014JB010970
Borromeo L, Andò S, France-Lanord C, Coletti G, Hahn A, Garzanti E (2019) Provenance of Bengal shelf sediments: 1 Mineralogy and Geochemistry of Silt. Minerals 9(10):640
Chamley H (1989) Clay sedimentology. Springer, Berlin. https://doi.org/10.1007/978-3-642-85916
Chaudhri RS, Gill GTS (1983) Clay mineralogy of the Siwalik Group of Simla Hills, northwestern Himalaya. J Geol Soc India 24:159–165
Chen LH, MIAO X, YU Z (1986) Application of scanning electron microscope on geology. Sience Press, Beijing
Chen Q, Liu Z, Kissel C (2017) Clay mineralogical and geochemical proxies of the East Asian summer monsoon evolution in the South China Sea during Late Quaternary. Sci Rep 7:1–9. https://doi.org/10.1038/srep42083
Costantini EA, Carnicelli S, Sauer D, Priori S, Andreetta A, Kadereit A, Lorenzetti R (2018) Loess in Italy: genesis, characteristics and occurrence. CATENA 168:14–33
Cox R, Lowe DR, Cullers RL (1995) The influence of sediment recycling and basement composition on evolution of mudrock chemistry in the southwestern United States. Geochim Cosmochim Acta 59:2919–2940. https://doi.org/10.1016/0016-7037(95)00185-9
Delcaillau B (1992) Les Siwaliks du Népal oriental. Presses du CNRS
Dhital M (2015) Geology of the Nepal Himalaya: regional perspective of the classic collided orogen
Ding Z, Sun J, Rutter NW, Rokosh D, Liu T (1999) Changes in sand content of loess deposits along a north–south transect of the Chinese Loess Plateau and the implications for desert variations. Quatern Res 52(1):56–62
Dodonov AE, Baiguzina LL (1995) Loess stratigraphy of Central Asia: palaeoclimatic and palaeoenvironmental aspects. Quat Sci Rev 14:707–720
Enzel Y, Amit R, Crouvi O, Porat N (2010) Abrasion-derived sediments under intensified winds at the latest Pleistocene leading edge of the advancing Sinai-Negev erg. Quat Res 74:121–131. https://doi.org/10.1016/j.yqres.2010.04.002
Fedo CM, Nesbitt HW, Young GM (1995) Unravelling the effects of potassium metasomatism in sedimentary rocks and paleosols, with implications for paleoweathering conditions and provenance. Geology 23:921–924. https://doi.org/10.1130/0091-7613(1995)023%3c0921:UTEOPM%3e2.3.CO
Gansser A (1974) Himalaya. Geological Society, London, Special Publications, vol 4, issue 1, pp 267–278
Guggenberger G, Bäumler R, Zech W (1998) Weathering of soils developed in eolian material overlying glacial deposits in Eastern Nepal. Soil Sci 163:325–337
Harnois L (1988) The CIW index: a new chemical index of weathering. Sed Geol 55(3):319–322
Heller F, Tungsheng L (1984) Magnetism of Chinese loess deposits. Geophys J Int 77:125–141. https://doi.org/10.1111/j.1365-246X.1984.tb01928.x
Herzschuh U, Winter K, Wünnemann B, Li S (2006) A general cooling trend on the central Tibetan Plateau throughout the Holocene recorded by the Lake Zigetang pollen spectra. Quat Int 154–155:113–121. https://doi.org/10.1016/j.quaint.2006.02.005
Huang Y, Xiao J, Xiang R, Liu S, Khokiattiwong S, Kornkanitnan N, Fan J, Wen R, Zhang S, Liu J (2020) Holocene Indian Summer Monsoon variations inferred from end-member modeling of sediment grain size in the Andaman Sea. Quatern Int 558:28–38
Jin Z, Cao J, Wu J, Wang S (2006) A Rb/Sr record of catchment weathering response to Holocene climate change in Inner Mongolia. Earth Surf Process Landforms 31:285–291. https://doi.org/10.1002/esp.1243

Jones SC, Pal JN (2009) The Palaeolithic of the Middle Son valley, north-central India: changes in hominin lithic technology and behaviour during the Upper Pleistocene. J Anthropol Archaeol 28(3):323–341
Khanal NR, Shrestha M, Ghimire M (2007) Preparing for flood disaster: mapping and assessing hazard in the Ratu Watershed, Nepal, International Centre for Integrated Mountain Development (ICIMOD)
Kotlia BS, Singh AK, Joshi LM, Dhaila BS (2015) Precipitation variability in the Indian Central Himalaya during last ca. 4,000 years inferred from a speleothem record: impact of Indian Summer Monsoon (ISM) and Westerlies. Quat Int 371:244–253. https://doi.org/10.1016/j.quaint.2014.10.066
Kukla G (1987) Loess stratigraphy in central China. Quat Sci Rev 6:191–219. https://doi.org/10.1016/0277-3791(87)90004-7
Laudari R, Sapkota B, Banskota K (2018) Validation of wind resource in 14 locations of Nepal. Renew Energy 119:777–786. https://doi.org/10.1016/j.renene.2017.10.068
Lehmkuhl F, Schulte P, Zhao H, Hülle D, Protze J, Stauch G (2014) Timing and spatial distribution of loess and loess-like sediments in the mountain areas of the northeastern Tibetan Plateau. CATENA 117:23–33. https://doi.org/10.1016/j.catena.2013.06.008
Leipe C, Demske D, Tarasov PE (2014) A Holocene pollen record from the northwestern Himalayan lake Tso Moriri: implications for palaeoclimatic and archaeological research. Quat Int 348:93–112. https://doi.org/10.1016/j.quaint.2013.05.005
Li Y, Zhao J, Li B (2017) Loess and loess geohazards in China. CRC Press
Li Y, Shi W, Aydin A, Beroya-Eitner MA, Gao G (2020) Loess genesis and worldwide distribution. Earth Sci Rev 201:102947
Liu Z, Wang H, Hantoro WS, Sathiamurthy E, Colin C, Zhao Y, Li J (2012) Climatic and tectonic controls on chemical weathering in tropical Southeast Asia (Malay Peninsula, Borneo, and Sumatra). Chem Geol 291:1–12. https://doi.org/10.1016/j.chemgeo.2011.11.015
Liu XM, Ma MM, Wu HB, Zhou ZB (2017) Identification of aeolian loess deposits on the Indo-Gangetic Plain (India) and their significance. Sci China Earth Sci 60(3):428–437
Liu Z, Colin C, Huang W, Phon Le K, Tong S, Chen Z, Trentesaux A (2007) Climatic and tectonic controls on weathering in south China and Indochina Peninsula: clay mineralogical and geochemical investigations from the Pearl, Red, and Mekong drainage basins. Geochem Geophys Geosyst 8. https://doi.org/10.1029/2006GC001490
Lone AM, Sharma S, Achyuthan H, Shukla AD, Shah RA, Sangode SJ, Fousiya AA (2023) Climatic implications of late Holocene loess and intervening paleosols, Southern Zanskar range, northwestern Himalaya. Phys Geogr 44(3):287–306
Lu H, Wang X, Miao X (2004) Geomorphologic evidence of phased uplift of the northeastern Qinghai-Tibet Plateau since 14 million years ago. Sci China Ser D Earth Sci Ed 47:822–833. https://doi.org/10.1360/03yd0315
Lupker M, France-Lanord C, Galy V, Lavé J, Gaillardet J, Gajurel AP, Guilmette C, Rahman M, Singh SK, Sinha R (2012) Predominant floodplain over mountain weathering of Himalayan sediments (Ganga basin). Geochim Cosmochim Acta 84:410–432
Lupker M, France-Lanord C, Galy V, Lavé J, Kudrass H (2013) Increasing chemical weathering in the Himalayan system since the last glacial maximum. Earth Planet Sci Lett 365:243–252
Maher BA, Thompson R (1992) Paleoclimatic significance of the mineral magnetic record of the Chinese loess and paleosols. Quat Res 37:155–170. https://doi.org/10.1016/0033-5894(92)90079-X
McLennan SM, Taylor SR, Eriksson KA (1983) Geochemistry of Archean shales from the Pilbara Supergroup, western Australia. Geochimica et Cosmochimica Acta 47(7):1211–1222
McLennan SM (1993) Weathering and global denudation. J Geol 101(2):295–303
Medlicott HB (1864) On the geological structure and relations of the southern portion of the Himalayan range between the rivers Ganges and Ravee. Mem Geol Surv India 3:1–212
Mir JA, Dar RA, Vinnepand M, Laag C, Rolf C, Zeeden C (2022) Environmental reconstruction potentials of Loess-Paleosol-Sequences in Kashmir through high-resolution proxy data. Palaeogeogr Palaeoclimatol Palaeoecol 601:111100
Mohindra R, Parkash B (1994) Geomorphology and Neotectonic Activity of Time Gandak Mega-Fan and Adjoining Areas, Middle Gangetic Plains. Geol Soc India 43(2):149–157
Moosavirad SM, Janardhana MR, Sethumadhav MS, Moghadam MR, Shankara M (2011) Geochemistry of lower Jurassic shales of the Shemshak Formation, Kerman Province, Central Iran: provenance, source weathering and tectonic setting. Chem Erde 71:279–288. https://doi.org/10.1016/j.chemer.2010.10.001
Muhs DR (2018) The geochemistry of loess: Asian and North American deposits compared. J Asian Earth Sci 155:81–115
Murray AS, Wintle AG (2000) Luminescence dating of quartz using an improved single-aliquot regenerative-dose protocol. Radiat Meas 32:57–73. https://doi.org/10.1016/S1350-4487(99)00253-X
Nesbitt H, Young GM (1982) Early Proterozoic climates and plate motions inferred from major element chemistry of lutites. Nature 299(5885):715–717
Ohata T, Higuchi K, Ikegami K (1981) Mountain-valley wind system in the Khumbu Himal, East Nepal. J Meteorol Soc Japan Ser II 59:753–762. https://doi.org/10.2151/jmsj1965.59.5_753
Owen LA, Finkel RC, Haizhou M, Barnard PL (2006) Late Quaternary landscape evolution in the Kunlun Mountains and Qaidam Basin, Northern Tibet: a framework for examining the links between glaciation, lake level changes and alluvial fan formation. Quat Int 154–155:73–86. https://doi.org/10.1016/j.quaint.2006.02.008
Pant RK (1993) Spread of loess and march of desert in western India. Curr Sci 64(11–12):841–847
Phadtare NR (2000) Sharp decrease in summer monsoon strength 4000–3500 cal yr B.P. in the central Higher Himalaya of India based on pollen evidence from alpine peat. Quat Res 53:122–129. https://doi.org/10.1006/qres.1999.2108
Porter SC (2001) Chinese loess record of monsoon climate during the last glacial-interglacial cycle. Earth-Sci Rev 54:115–128. https://doi.org/10.1016/S0012-8252(01)00043-5
Prescott JR, Hutton JT (1994) Cosmic ray contributions to dose rates for luminescence and ESR dating: large depths and long-term time variations. Radiat Meas 23(2–3):497–500. https://doi.org/10.1016/1350-4487(94)90086-8
Pye K (1987) Aeolian dust and dust deposits. Academic Press, London
Pye K (1995) The nature, origin and accumulation of loess. Quatern Sci Rev 14(7–8):653–667
Raiverman V, Suresh N (1997) Clay mineral distribution in the Cenozoic sequence of the western Himalayan Foothills. J Indian Assoc Sediment 16:63–75
Ramage C (1971) Monsoon meteorology. Academic Press, New York
Ramisch A, Lockot G, Haberzettl T, Hartmann K, Kuhn G, Lehmkuhl F, Schimpf S, Schulte P, Stauch G, Wang R, Wünnemann B (2016) A persistent northern boundary of Indian Summer Monsoon precipitation over Central Asia during the Holocene. Sci Rep 6(1):1–7
Ranjan N, Banerjee DM (2009) Central Himalayan crystallines as the primary source for the sandstone-mudstone suites of the Siwalik Group: new geochemical evidence. Gondwana Res 16:687–696. https://doi.org/10.1016/j.gr.2009.07.005
Rashid H, Flower BP, Poore RZ, Quinn TM (2007) A∼ 25 ka Indian Ocean monsoon variability record from the Andaman Sea. Quatern Sci Rev 26(19–21):2586–2597
Roberts HM (2007) Assessing the effectiveness of the double-SAR protocol in isolating a luminescence signal dominated by quartz. Radiat Meas 42:1627–1636. https://doi.org/10.1016/j.radmeas.2007.09.010
Sang PN, Liu Z, Zhao Y, Zhao X, Pha PD, Van Long H (2018) Chemical weathering in central Vietnam from clay mineralogy and major-element geochemistry of sedimentary rocks and river sediments. Heliyon 4. https://doi.org/10.1016/j.heliyon.2018.e00710
Scull P, Schaetzl RJ (2011) Using PCA to characterize and differentiate loess deposits in Wisconsin and Upper Michigan, USA. Geomorphology 127(3–4):143–155
Shen C (2003) Millennial-scale variations and centennial-scale events in the Southwest Asian monsoon: pollen evidence from Tibet. Louisiana State University
Shen C, Kam-biu L, Tang L, Overpeck JT (2006) Quantitative relationships between modern pollen rain and climate in the Tibetan Plateau. Rev Palaeobot Palynol 140:61–77. https://doi.org/10.1016/j.revpalbo.2006.03.001
Sinha S, Islam R, Ghosh SK, Kumar R, Sangode SJ (2007) Geochemistry of Neogene Siwalik mudstones along Punjab re-entrant, India: implications

for source-area weathering, provenance and tectonic setting. Curr Sci. https://doi.org/10.2307/24097629
Sinha R, Ahmad J, Gaurav K, Morin G (2014) Shallow subsurface stratigraphy and alluvial architecture of the Kosi and Gandak megafans in the Himalayan foreland basin, India. Sed Geol 301:133–149
Stauch G, IJmker J, Pötsch S, Zhao H, Hilgers A, Diekmann B, Dietze E, Hartmann K, Opitz S, Wünnemann B, Lehmkuhl F (2012) Aeolian sediments on the north-eastern Tibetan Plateau. Quat Sci Rev 57:71–84. https://doi.org/10.1016/j.quascirev.2012.10.001
Sun JM (2002a) Provenance and forming mechanisms of the loess sediments on the high mountain regions of northwestern China. Quat Res 58:341–351
Sun J (2002b) Provenance of loess material and formation of loess deposits on the Chinese Loess Plateau. Earth Planet Sci Lett 203:845–859. https://doi.org/10.1016/S0012-821X(02)00921-4
Sun J, Li SH, Muhs DR, Li B (2007) Loess sedimentation in Tibet: provenance, processes, and link with Quaternary glaciations. Quat Sci Rev 26:2265–2280. https://doi.org/10.1016/j.quascirev.2007.05.003
Suresh N, Ghosh SK, Kumar R, Sangode SJ (2004) Clay-mineral distribution patterns in late Neogene fluvial sediments of the Subathu sub-basin, central sector of Himalayan foreland basin: implications for provenance and climate. Sediment Geol 163:265–278. https://doi.org/10.1016/j.sedgeo.2003.07.006
Tamrakar KN, Syangbo KD (2014) Petrography and provenance of the Siwalik Group sandstones from the Main Boundary Thrust region, Samari River area, Central Nepal, sub-Himalaya. Boletín Geol 36:25–44
Tartari G, Verza G, Bertolami L (1998) Meteorological data at the Pyramid Observatory Laboratory. Mem Ist Ital Idrobiol 57:23–40
Thiry M (2000) Palaeoclimatic interpretation of clay minerals in marine deposits: an outlook from the continental origin. Earth Sci Rev 49:201–221. https://doi.org/10.1016/S0012-8252(99)00054-9
Thomas J, Kar A, Kailath A, Für NJ-Z (1999) Late Pleistocene-Holocene history of aeolian accumulation in the Thar Desert, India. Z Geomorphol 116:181–194
Tokuoka T, Takeda S, Yoshida M, Upreti BN (1988) The Churia (Siwalik) Group in the western part of the Arung Khola area, west central Nepal. Mem Fac Sci 22:131–140
Tripathi J, Bock B, Rajamani V (2004) Is river Ghaggar, Saraswati. Curr Sci 87:1141–1145
Vandenberghe J (2013) Grain size of fine-grained windblown sediment: a powerful proxy for process identification. Earth Sci Rev. https://doi.org/10.1016/j.earscirev.2013.03.001
Vandenberghe J, Sun Y, Wang X, Abels HA, Liu X (2018) Grain-size characterization of reworked fine-grained aeolian deposits. Earth Sci Rev. https://doi.org/10.1016/j.earscirev.2017.11.005
Velbel MA (2007) Surface textures and dissolution processes of heavy minerals in the sedimentary cycle: examples from pyroxenes and amphiboles. Development Sedimentol 58:113–150
Vos K, Vandenberghe N, Elsen J (2014) Surface textural analysis of quartz grains by scanning electron microscopy (SEM): From sample preparation to environmental interpretation. Earth-Sci Rev 128:93–104
Wang J, Chen Z, Gao Q, Grapes R, Peng Z, Chen G (2018) Late Pleistocene loess-like deposits in the coastal area of south China. Catena 167:305–318
Wang Y, Zhang E, Sun W, Chang J, Liu X, Ni Z, Ning D (2019) Holocene evolution of the Indian summer monsoon inferred from a lacustrine record of Lake Wuxu, south-east Tibetan Plateau. J Quat Sci 34(6):463–474
Yuan D, Cheng H, Edwards RL, Dykoski CA, Kelly MJ, Zhang M, Qing J, Lin Y, Wang Y, Wu J, Dorale JA (2004) Timing, duration, and transitions of the last interglacial Asian monsoon. Science 304(5670):575–578
Zárate MA (2003) Loess of southern South America. Quatern Sci Rev 22(18–19):1987–2006
Zhang J, Feng JL, Hu G, Wang J, Yang Y, Lin Y, Jiang T, Zhu L (2015) Holocene proglacial loess in the Ranwu valley, southeastern Tibet, and its paleoclimatic implications. Quat Int 372:9–22. https://doi.org/10.1016/j.quaint.2014.04.016
Zhao Y, Yu Z (2012) Vegetation response to Holocene climate change in East Asian monsoon-margin region. Earth Sci Rev. https://doi.org/10.1016/j.earscirev.2012.03.001
Zhao Y, Yu Z, Chen F, Zhang J, Yang B (2009) Vegetation response to Holocene climate change in monsoon-influenced region of China. Earth Sci Rev. https://doi.org/10.1016/j.earscirev.2009.10.007
Zhou W, Yu S-Y, Burr GS, Kukla GJ, Jull AJT, Xian F, Xiao J, Colman SM, Yu H, Liu Z, Kong X (2010) Postglacial changes in the Asian summer monsoon system: a pollen record from the eastern margin of the Tibetan Plateau. Boreas 39:528–539. https://doi.org/10.1111/j.1502-3885.2010.00150.x
Zimmerman DW (1971) Thermoluminescent dating using fine grains from pottery. Archaeometry 13:29–52. https://doi.org/10.1111/j.1475-4754.1971.tb00028.x

Publisher's Note